

Robust Segmentation Models using an Uncertainty Slice Sampling Based Annotation Workflow

GRZEGORZ CHLEBUS^{1,2}, ANDREA SCHENK¹, HORST K. HAHN^{1,3},
BRAM VAN GINNEKEN^{1,2}, AND HANS MEINE^{1,4}

¹Fraunhofer Institute for Digital Medicine MEVIS, 28359 Bremen, Germany

²Diagnostic Image Analysis Group, Department of Medical Imaging, Radboud University Medical Center, 6525 Nijmegen, The Netherlands

³Jacobs University, 28759 Bremen, Germany

⁴University of Bremen, Medical Image Computing Group, 28359 Bremen, Germany

Corresponding author: Grzegorz Chlebus (e-mail: grzegorz.chlebus@mevis.fraunhofer.de).

arXiv:2109.14879v1 [cs.CV] 30 Sep 2021

ABSTRACT Semantic segmentation neural networks require pixel-level annotations in large quantities to achieve a good performance. In the medical domain, such annotations are expensive, because they are time-consuming and require expert knowledge. Active learning optimizes the annotation effort by devising strategies to select cases for labeling that are most informative to the model.

In this work, we propose an uncertainty slice sampling (USS) strategy for semantic segmentation of 3D medical volumes that selects 2D image slices for annotation and compare it with various other strategies. We demonstrate the efficiency of USS on a CT liver segmentation task using multi-site data. After five iterations, the training data resulting from USS consisted of 2410 slices (4% of all slices in the data pool) compared to 8121 (13%), 8641 (14%), and 3730 (6%) for uncertainty volume (UVS), random volume (RVS), and random slice (RSS) sampling, respectively.

Despite being trained on the smallest amount of data, the model based on the USS strategy evaluated on 234 test volumes significantly outperformed models trained according to other strategies and achieved a mean Dice index of 0.964, a relative volume error of 4.2%, a mean surface distance of 1.35 mm, and a Hausdorff distance of 23.4 mm. This was only slightly inferior to 0.967, 3.8%, 1.18 mm, and 22.9 mm achieved by a model trained on all available data, but the robustness analysis using the 5th percentile of Dice and the 95th percentile of the remaining metrics demonstrated that USS resulted not only in the most robust model compared to other sampling schemes, but also outperformed the model trained on all data according to Dice (0.946 vs. 0.945) and mean surface distance (1.92 mm vs. 2.03 mm).

INDEX TERMS Active learning, convolutional neural network, deep learning, segmentation, uncertainty sampling.

I. INTRODUCTION

SEMANTIC segmentation of medical images plays a key role in many treatment planning workflows. Over the recent years, segmentation algorithms utilizing deep neural networks have provided state-of-the-art results for many segmentation tasks [1]–[3]. Training of such systems typically requires large data sets with pixel-level annotations to achieve good performance. In the medical domain, such annotations require expert knowledge and are time-consuming, and thus, are expensive to obtain. Although many pre-trained segmentation models are available, it is known that neural networks underperform when applied to data coming from different sites or imaging protocols [4], [5]. Therefore, to get

the optimal performance, training on annotated target data is recommended.

Active learning is a prominent technique for the optimization of annotation effort [6]. It aims to design an optimal way to select training data resulting in high performance with low annotation cost. Numerous active learning algorithms are pool-based, meaning that they employ query strategies to choose samples from the unlabeled data pool. Pool-based query strategies typically take the model's uncertainty [7], [8], sample representativeness [9], or both of them [10], [11] into account.

Smailagic et al. proposed a strategy for a classification problem that uses predictive entropy to identify most uncer-

tain examples in the data pool [11]. Among these examples, those that maximize the distance to the training set in a feature space defined by one of the model layers are selected. Addition of the distance maximization criterion allowed for a 32% reduction in the number of required labeled examples. A similar approach for a segmentation task was demonstrated by Yang *et al.* [10], where an ensemble was used to pick uncertain cases defined as ones with the highest average per-pixel variance. Additionally, examples with the highest representativeness according to the cosine similarity distance based on descriptors obtained from the model were picked for manual annotation. Models trained using this approach achieved a state-of-the-art performance using only 50% of the training data.

Wang *et al.* introduced cost-effective active learning for image classification where in addition to manually labeled uncertain cases, ones with high confidence are pseudo-labeled by the model and added to the training set with no annotation effort [7]. A variational adversarial query strategy was proposed by Sinha *et al.* that employs a discriminator network to differentiate between labeled and unlabeled examples [12]. This approach chooses points that are not well represented in the labeled set without the need for uncertainty measurement on the main task.

While most of the pool-based active learning research focuses on uncertainty quantification and example representativeness, little attention was given to the incorporation of partial annotations into the workflow. Partial annotations are particularly relevant for semantic segmentation tasks as they can result in a substantial annotation effort reduction [13], especially when dealing with volumetric data. In this work, we propose an uncertainty slice sampling (USS) query strategy to optimize the annotation workflow of 3D medical images. Our strategy selects 2D image slices for annotation from a pool of unlabeled 3D volumes using predictive entropy as the uncertainty measure. We see this as a way to increase the variability of the training set without the need for explicit modeling of example representativeness. We show the efficiency of our strategy on a CT liver segmentation task using multi-site data. We designed our experiments in such a way that they use a comparable annotation effort. We analyze the proposed strategy together with several alternatives: uncertainty volume sampling (UVS), random volume sampling (RVS), and random slice sampling (RSS).

II. METHODS

A. NEURAL NETWORK ARCHITECTURE

We use a 3D anisotropic u-net (au-net) architecture (see Fig. 1) that is a modified version of the commonly used encoder-decoder u-net segmentation network design [14]. The model works on five resolution levels. In the upper two levels, convolutional layers work only along x and y spatial dimensions and the remaining levels contain separable 3D convolutions to minimize the number of trainable parameters. Each convolution layer is followed by batch normalization [15] and ReLU. Max pooling (transposed 3D conv) layers

are used in the encoder (decoder) for transitioning down (up) between resolution levels. Dropout layer [16] with a drop rate $p = 0.25$ is placed at each resolution level in the decoder path to prevent overfitting and facilitate Monte Carlo (MC) sampling used for the uncertainty estimation.

B. TRAINING SETUP

All models are trained using a mini-batch size of 2 using $180 \times 180 \times 4$ image patches that are padded (reflect mode) on each side with 92 voxels along x and y and 20 along z spatial dimension to account for valid convolutions. Optimization is done using the Adam optimizer with 10^{-5} learning rate. The model is applied to the validation data every 1000 iterations and the best model according to the Jaccard index is used for the final evaluation.

Stratified patch sampling is employed to speed up the training by ensuring that at least one patch in a mini-batch contains liver pixels. We use a weighted soft dice loss to enable training with partially annotated patches (required for slice sampling strategies) [17]:

$$L_{DSC} = 1 - \frac{2 \sum_i w_i y_i p_i}{\sum_i w_i y_i + \sum_i w_i p_i} \quad (1)$$

where y_i is i th voxel label (1 - liver, 0 - background), p_i is the output probability of the liver class, w_i is 1 for annotated voxels and 0 otherwise, and i runs over all voxels in a mini-batch.

C. DATA PREPROCESSING

For training, all CT volumes were rescaled into Hounsfield units and resampled to $1.0 \text{ mm} \times 1.0 \text{ mm} \times 1.5 \text{ mm}$ voxel size.

D. UNCERTAINTY ESTIMATION

Several uncertainty estimation methods for segmentation models have been proposed including volume variation coefficient [18], prediction variance [10], predictive entropy, and mutual information [19]. These methods require multiple samples, which are typically obtained from an ensemble or via MC dropout [20]. In our work, we use the predictive entropy as the uncertainty measure per voxel \mathbf{x} :

$$U(\mathbf{x}) = - \sum_c \left(\frac{1}{n} \sum_n p_n(y = c|\mathbf{x}) \right) \ln \left(\frac{1}{n} \sum_n p_n(y = c|\mathbf{x}) \right) \quad (2)$$

where c is the number of classes, n is the number of samples, $p_n(y = c|\mathbf{x})$ is the softmax probability of input \mathbf{x} belonging to class c in the n th sample. In our experiments, we obtain $n = 20$ samples via MC dropout to capture the epistemic uncertainty accounting for the uncertainty in the model parameters [21].

Volume-level uncertainty Similarly to [22], we use the average of the voxel-wise predictive entropy as a measure of the uncertainty at a volume-level. We exclude voxels outside

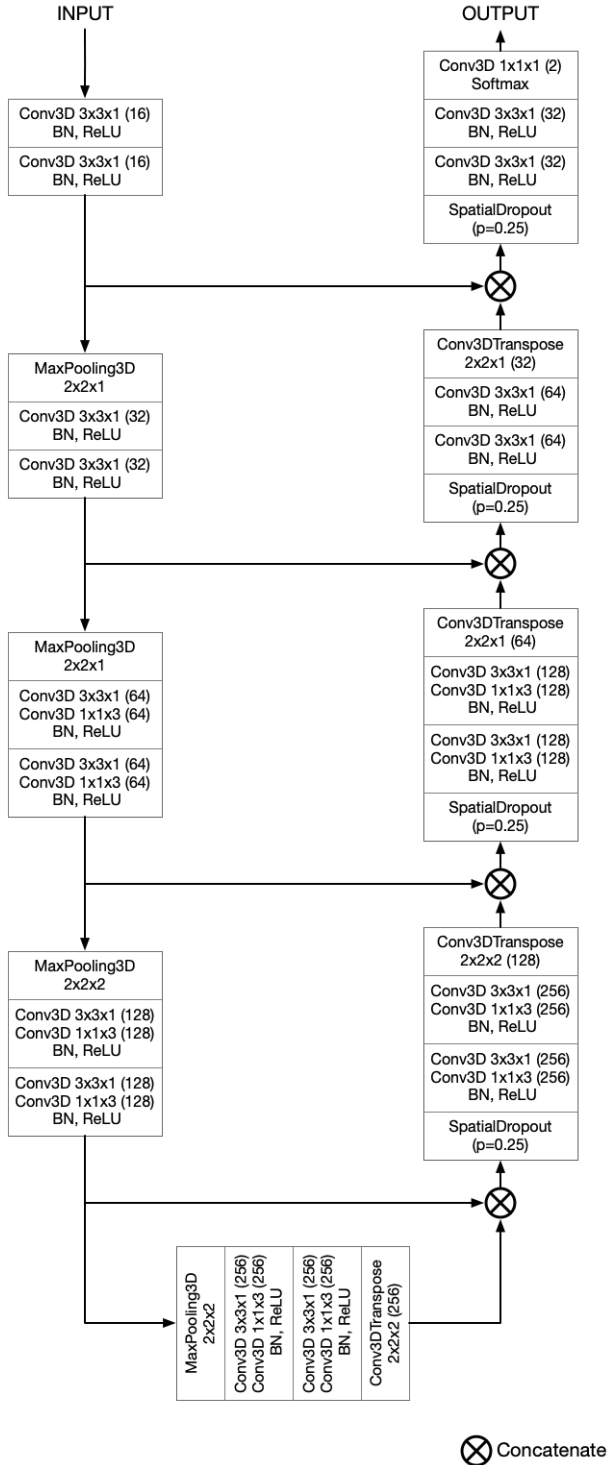


FIGURE 1: Anisotropic u-net (au-net) architecture. The model has 4 975 346 trainable parameters.

of a dilated liver mask ($11 \times 11 \times 11$ kernel) for volume size invariance.

Slice-level uncertainty is computed as the average of the predictive entropy for all voxels belonging to a given slice. Contrary to the volume-level uncertainty, we compute the

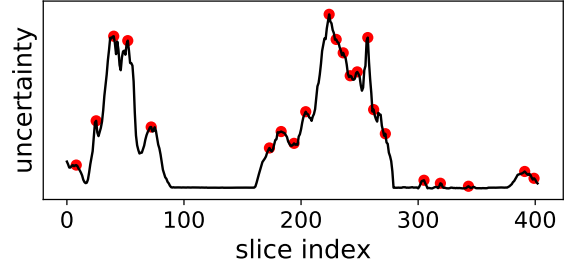


FIGURE 2: Slice uncertainty profile. The red dots correspond to slice candidates available to the uncertainty slice sampling strategy.

average over all voxels, because the slice-level measure is less sensitive to liver size variability.

E. QUERY STRATEGIES

Query strategies select which samples from the unlabeled data pool should be annotated and added to the training set. In our study, we investigate two orthogonal dimensions of query strategies: i) selection of 3D image volumes vs. 2D image slices and ii) random vs. uncertainty-based sampling. These dimensions define four sampling strategies that work as follows:

Uncertainty Volume Sampling (UVS) selects volumes with the biggest volume-level uncertainty.

Random Volume Sampling (RVS) selects volumes at random.

Uncertainty Slice Sampling (USS) selects slice candidates with the biggest slice-level uncertainty. A slice candidate is extracted from a slice-level uncertainty vs. slice index curve using local maxima (see Fig. 2). We require a minimum distance between peaks to be five slices to avoid selecting neighboring slices.

Random Slice Sampling (RSS) selects slices at random.

F. EVALUATION METRICS

We evaluate the segmentation quality with four commonly used metrics: Dice index (DICE), relative volume error (RVE), mean surface distance (MSD), and Hausdorff distance (HD) [23]. These metrics are defined as follows:

$$\text{DICE}(X, Y) = \frac{2|X \cap Y|}{|X| + |Y|} \quad (3)$$

$$\text{RVE}(X, Y) = \frac{|V_X - V_Y|}{V_Y} \cdot 100\% \quad (4)$$

$$\text{MSD}(X, Y) = \frac{1}{2N} \left(\sum_{x \in X} \min_{y \in Y} d(x, y) + \sum_{y \in Y} \min_{x \in X} d(x, y) \right) \quad (5)$$

$$\text{HD}(X, Y) = \max \left\{ \sup_{x \in X} \inf_{y \in Y} d(x, y), \sup_{y \in Y} \inf_{x \in X} d(x, y) \right\} \quad (6)$$

where V_X and V_Y are volumes of the test and the reference object, respectively, and $d(x, y)$ is the Euclidean distance between points x and y .

In addition to reporting evaluation results on the test set using mean \pm standard deviation, we report the 5th percentile for the DICE and the 95th percentile for the remaining metrics. We use these percentile-based measures to assess the impact of investigated query strategies on models' robustness.

III. DATA

In this work, we simulate the active learning-based annotation workflow by using abdominal CT volumes with reference liver segmentations. To increase the statistical power of our study, we decided to use imaging data coming from five datasets containing together 484 CT volumes. Three of them are proprietary and were obtained via cooperation with clinical partners: Yokohama City University, Yokohama, Japan (*Yokohama*), Städtisches Klinikum Dresden, Dresden, Germany (*Dresden*), and Radboud University Clinical Center, Nijmegen, the Netherlands (*Rumc*). Two remaining two (*LiTS*, *CHAOS*) come from publicly organized challenges [3], [24]. Reference liver segmentations for the proprietary data were created manually by experienced clinical experts using dedicated annotation software [25]. The challenge data comes with training liver masks that we used as reference segmentations. In the case of *LiTS* data, 65 out of 131 volumes were excluded by our medical experts due to a poor segmentation quality. The combined dataset was divided into three subsets containing 240, 10, and 234 cases that were used as data pool, validation set, and test set, respectively. The reader is referred to Tab. 1 for more details.

IV. EXPERIMENTS

Our goal was to compare the investigated query strategies by keeping the required annotation effort at a comparable level. To this end, we made the following assumptions w.r.t. the annotation effort:

- 1) the effort required for annotation of N slices with liver in one image volume is approx. equal to the annotation effort of $N/3$ slices with liver coming from different volumes;
- 2) the effort required for a slice without a liver is negligible in comparison to liver slices.

The first assumption was derived empirically from an observation that for segmentation of one volume one needs to manually draw contours on average on every third slice when using modern segmentation tools with interpolation functionality.

A. QUERY STRATEGY COMPARISON

To evaluate the efficiency of the investigated query strategies, we performed five active learning iterations and compared models after each iteration. We used a model trained on five fully annotated cases as the initial model. In each iteration, we trained a model from scratch and we used the

best model according to the validation score for evaluation and uncertainty estimation. All models were trained for a max of 30 epochs, which is short enough to guarantee that model training and selection of cases for annotation can be performed overnight.

For volume sampling strategies we added five volumes to the training set in each iteration and we denote by $\tilde{N}_S^{\text{liver}}$ the average count of liver slices added in each UVS iteration. Based on our assumption w.r.t. the annotation effort, in the USS strategy we added $N_S = \tilde{N}_S^{\text{liver}}/3$ slices in each iteration, whereas in the RSS we sampled random slices until N_S liver slices were selected.

B. CONVERGED MODELS COMPARISON

To evaluate the representativeness of training sets obtained with the investigated query strategies after five active learning iterations, we compared models trained on these training sets until convergence. This was motivated by the fact that, for some of the models, 30 epochs were not long enough to converge.

V. RESULTS

A. ANNOTATION EFFORT

The initial model was trained using five fully annotated volumes accounting for a total of 1410 (501) annotated slices (liver slices). On average, 1342 (576) and 1446 (558) slices were annotated in each UVS and RVS iteration, respectively. In USS and RSS iterations, we sampled $N_S = 200$ ($576/3 \approx 200$) slices. Consequently, in the last 5th and final iteration, the models were trained using 13% (13%), 14% (12%), 4% (5%), and 6% (6%) of all slices (liver slices) available in the data pool for the UVS, RVS, USS, and RSS strategy, respectively. More details can be found in Tab. 2.

B. QUERY STRATEGY COMPARISON

For all strategies, an overall improvement in all segmentation metrics was observed over the course of active learning iterations (see Fig. 3). The mean performance of the initial model was 0.925, 7.87%, 2.94 mm, and 36.3 mm for DICE, RVE, MSD, and HD, respectively. The mean performance of models resulting from the fifth (last) iteration of the investigated query strategies was in the range of [0.956, 0.960], [3.98, 6.04]%, [1.4, 1.73] mm, and [25.6, 28.6] mm for DICE, RVE, MSD, and HD, respectively (see Tab. 4-7). The model obtained from the last iteration of the USS strategy was significantly better (Wilcoxon signed-rank test) than the models from the remaining strategies. When considering segmentation metrics across all five iterations, the USS strategy resulted in the best-performing model most of the time. Interestingly, this strategy produced the worst model according to all metrics in the first iteration, even failing to improve the initial model's performance for RVE and HD. None of the models trained with 4%-14% of the data was able to match the results of the model trained on the whole data pool that achieved on average 0.967 DICE, 3.8% RVE, 1.18 mm MSD, and 22.9 mm HD.

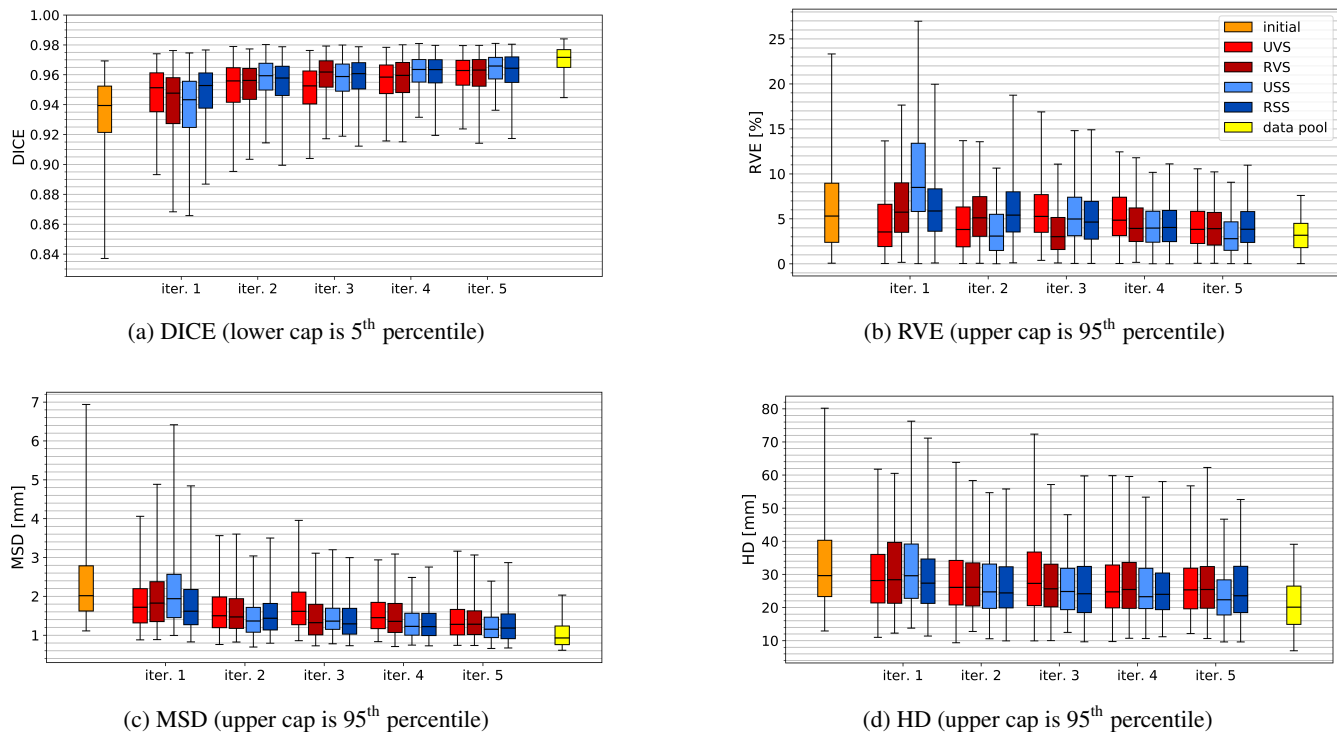


FIGURE 3: Box plots summarizing evaluation results for models trained throughout five active learning iterations. For reference, results of the initial and whole data pool models are included.

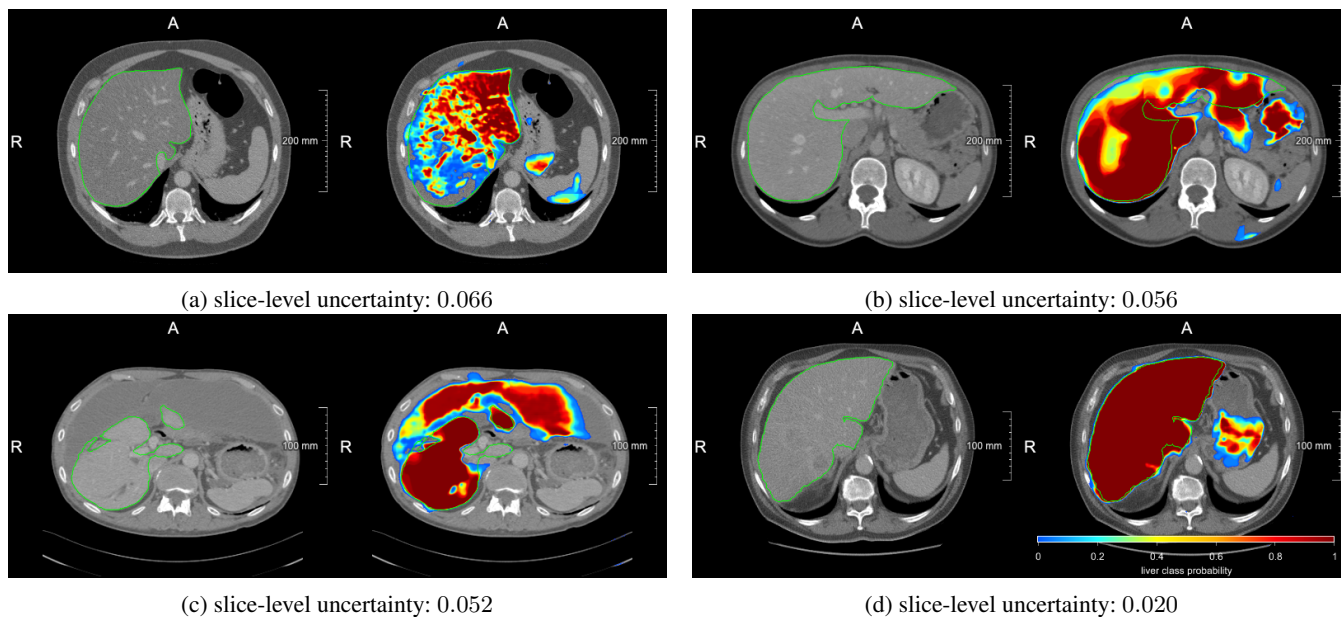
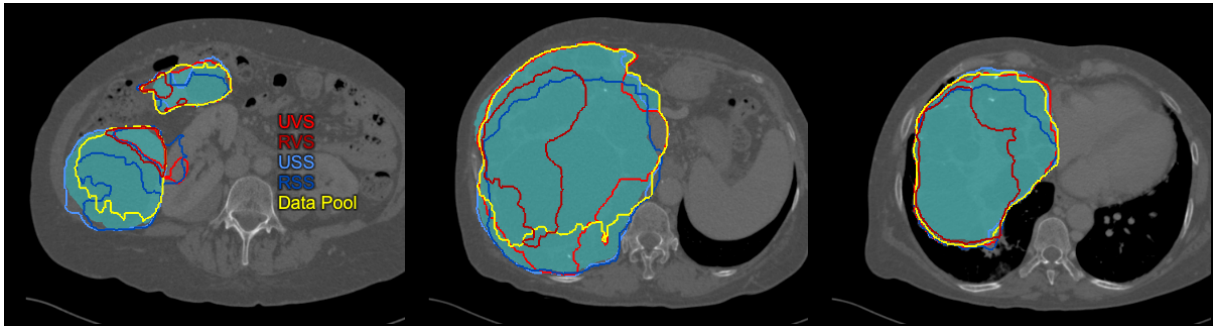
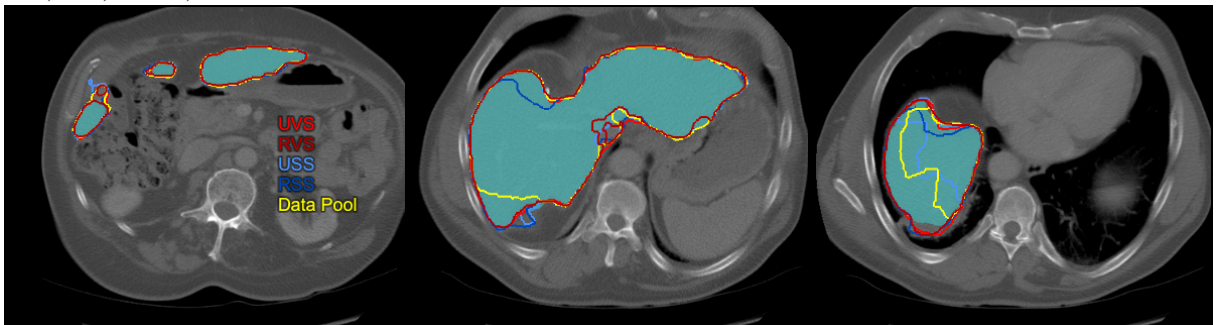


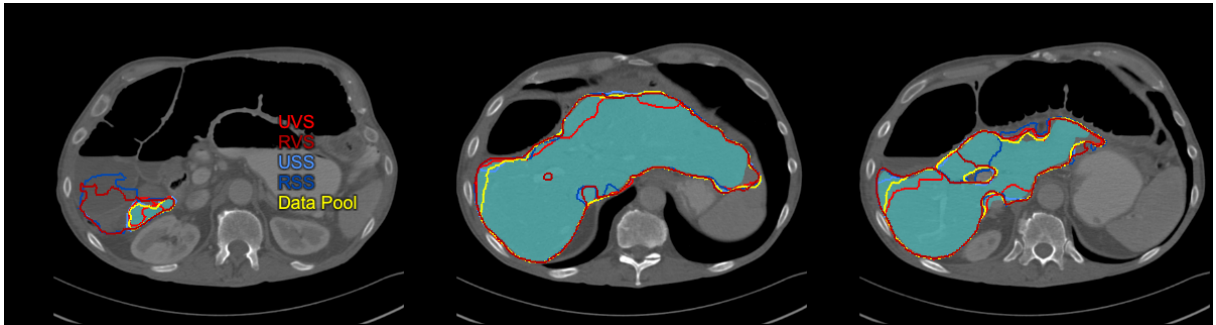
FIGURE 4: Examples of slices selected in the first USS iteration with overlaid liver reference segmentation (green contour) and model liver probability output (heatmap): (a)-(c) slices with the biggest slice level uncertainty, (d) slice with the lowest uncertainty among selected ones.



(a) Polycystic liver case where the USS strategy resulted in the best segmentation: *UVS* 0.83 Dice, 25.2% RVE, 8.0 mm MSD, 64 mm HD; *RVS* 0.53, 63.2%, 18.0 mm, 64 mm; *USS* 0.94, 5.2%, 3.2 mm, 59 mm; *RSS* 0.84, 21.7%, 8.7 mm, 65 mm; *Data Pool* 0.85, 24%, 8.3 mm, 64 mm.



(b) Case where UVS outperformed all models: *UVS* 0.96 Dice, 0.4% RVE, 1.1 mm MSD, 17 mm HD; *RVS* 0.96, 3.1%, 1.4 mm, 21 mm; *USS* 0.94, 5.6%, 1.5 mm, 24 mm; *RSS* 0.95, 2.5%, 1.4 mm, 22 mm; *Data Pool* 0.93, 9.1%, 2.1 mm, 32 mm.



(c) Case where both random strategies resulted in overestimation in the caudal liver region: *UVS* 0.91 Dice, 6.1% RVE, 2.4 mm MSD, 23 mm HD; *RVS* 0.93, 3.4%, 2.1 mm, 25 mm; *USS* 0.95, 1.0%, 1.5 mm, 17 mm; *RSS* 0.77, 41.0%, 23.3 mm, 141 mm; *Data Pool* 0.94, 0.2%, 1.7 mm, 21 mm.



(d) Case for which all strategies except RVS achieved very good segmentation performance: *UVS* 0.97 Dice, 0.1% RVE, 0.9 mm MSD, 18 mm HD; *RVS* 0.91, 11.8%, 2.9 mm, 36 mm; *USS* 0.96, 1.8%, 1.0 mm, 20 mm; *RSS* 0.97, 1.6%, 0.9 mm, 20 mm; *Data Pool* 0.97, 0.0%, 0.8 mm, 20 mm.

FIGURE 5: Representative examples presenting segmentation output of the converged models and the model trained on the whole data pool.

TABLE 1: Dataset details.

Dataset Name	#Volumes (pool/val/test)	Voxel Size [mm]	Resolution
Yokohama	218 (119/2/97)	[0.5-0.8]×[0.5-0.8]×[0.8-1.6]	512×512×[170-376]
Rumc	100 (46/2/52)	[0.6-1.0]×[0.6-1.0]×[0.7-1.5]	512×512×[378-1057]
Dresden	80 (36/2/42)	[0.6-0.9]×[0.6-0.9]×[0.5-5.0]	512×512×[71-1160]
LiTS	66 (31/2/33)	[0.6-1.0]×[0.6-1.0]×[0.7-5.0]	512×512×[74-987]
CHAOS	20 (8/2/10)	[0.6-0.8]×[0.6-0.8]×[1.0-2.0]	512×512×[81-266]

TABLE 2: Training data summary (annotated slices/annotated liver slices/unique patients) over the course of five active learning iteration for each investigated query strategy.

	UVS	RVS	USS	RSS
initial	1410/501/5			
iter. 1	2541/1045/10	3206/1070/10	1610/669/72	1873/701/195
iter. 2	3651/1537/15	4631/1608/15	1810/797/104	2323/901/233
iter. 3	5105/2224/20	5813/2150/20	2010/947/125	2790/1101/236
iter. 4	6941/2761/25	7094/2687/25	2210/1123/149	3278/1301/239
iter. 5	8121/3382/30	8641/3292/30	2410/1292/160	3730/1501/240
data pool	60513/26400/242			

TABLE 3: Training step count for models used for evaluation obtained using four investigated query strategies over five active learning iterations. For reference, data for the initial and data pool model is given.

	UVS	RVS	USS	RSS
initial	12 000			
iter. 1	35 000	37 000	40 000	46 000
iter. 2	61 000	64 000	61 000	67 000
iter. 3	80 000	83 000	71 000	94 000
iter. 4	75 000	85 000	91 000	117 000
iter. 5	119 000	98 000	98 000	139 000
iter. 5 (converged)	356 000	297 000	291 000	465 000
data pool	825 000			

For volume sampling strategies there is no clear difference between uncertainty-based and random sampling. In the case of slice sampling strategies, the uncertainty-based sampling resulted in a consistent improvement (excluding the first iteration) across all metrics.

C. CONVERGED MODELS COMPARISON

Training until convergence using data resulting from the fifth active learning iteration resulted in an improvement of all segmentation metrics across all query strategies with one exception of RVE metric for the USS strategy (see Tab. 8 and Fig. 6). The model trained on data resulting from the RSS strategy required the longest training time (465k iterations), whereas the USS model needed the fewest iterations (291k) compared to 825k iterations for the model trained on the whole data pool. Among the investigated strategies, the USS model had the best performance when compared to other models with most of the differences being significant. None of the models achieved comparable results to the whole data pool model, but we observed that the USS model resulted in

more robust segmentations than the whole data pool model according to the 5th percentile for DICE and the 95th percentile for MSD and HD metric.

To quantify the effect of uncertainty-based vs random sampling and slice vs volume sampling on the 5th percentile of DICE and 95th percentile of the remaining metrics we performed a quantile regression analysis using evaluation results of the converged models (Tab. 9). Uncertainty sampling resulted in a significant improvement w.r.t. random sampling equal to 0.012 for the 5th percentile of DICE and -0.41 for the 95th percentile of MSD. Similarly, changing from volume to slice sampling results in an increase of 0.012 in the 5th percentile DICE and a decrease of 0.48 in the 95th percentile of MSD. The effect on the remaining metrics did not pass our significance test (95% confidence interval included 0).

VI. DISCUSSION

In our work, we proposed the uncertainty slice sampling (USS) strategy in the context of pool-based active learning. Our strategy selects 2D image slices from a pool of 3D volumes using aggregated voxel-wise predictive entropy as the uncertainty measure. We evaluated the proposed strategy on a CT liver segmentation task and compared it with random slice sampling (RSS), uncertainty volume sampling (UVS), and random volume sampling (RVS) strategies. The model trained using the USS data (4% of available data) achieved significantly better results than the remaining strategies. Although after five active learning iterations the USS model was inferior in performance on average to the model trained on all available data, it provided more robust segmentation as measured by 5th DICE and 95th MSD metrics. We hypothesize that this can be attributed to differences in the training set composition. The training set resulting from the USS contains a bigger proportion of difficult/rare cases compared to the whole data-pool training set, which effectively causes that the model sees them more frequently during the training process. Fig. 5 shows exemplary outputs from the investigated models including two hard cases from the test set: a polycystic (Fig. 5a) and a resected (Fig. 5b) liver. We think that the robustness of the whole data pool model could be increased by employing a hard example mining during training to dynamically adjust the sampling rate of difficult examples [26], [27]. Selecting only uncertain cases in the course of active learning can overload the model with difficult examples causing a performance drop. This can be observed for the USS strategy after the first iteration (see Fig. 3, where the model performs substantially worse than its

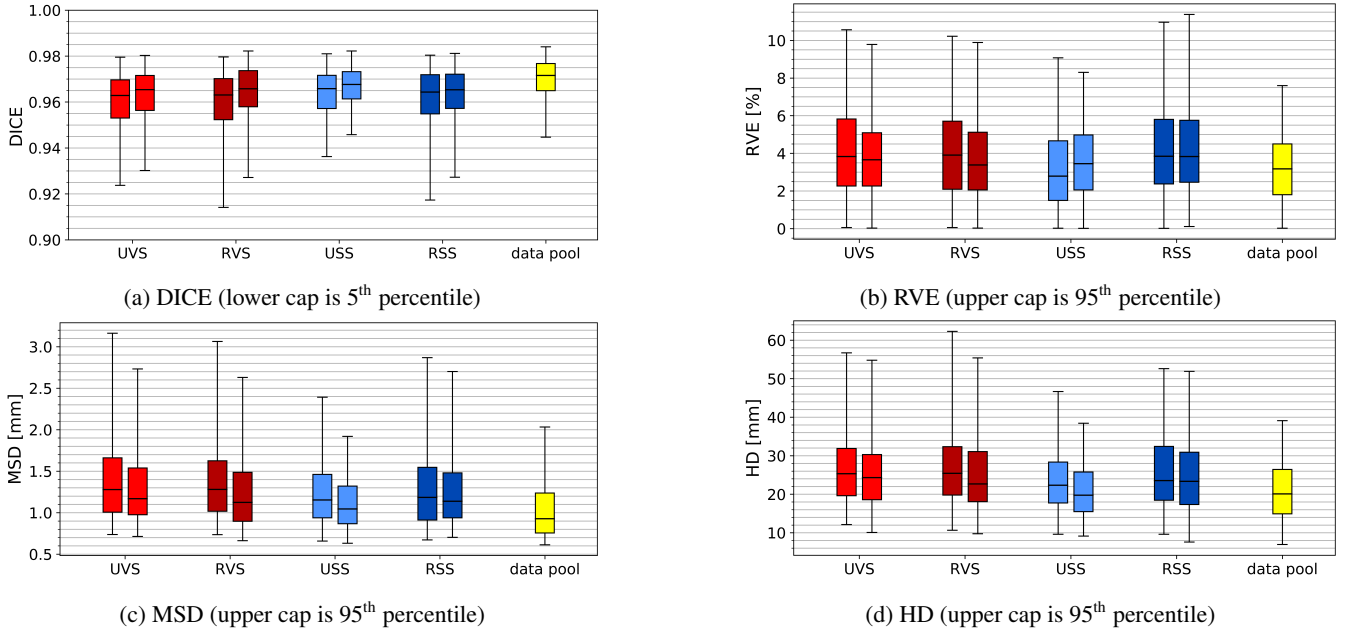


FIGURE 6: Box plots summarizing evaluation results for models trained for max of 30 epochs (left) and until convergence (right) using data from the fifth iteration. For reference, results of the whole data pool model are included.

TABLE 4: DICE for models trained using the investigated query strategies over five active learning iterations. For reference, results of the initial model and the model trained on the whole data pool are given.

	UVS	RVS	USS	RSS
initial		0.925 ± 0.068 (0.837)		
iter. 1	0.942 ± 0.037 (0.893)	0.937 ± 0.038 (0.868)***	0.932 ± 0.048 (0.866)***	0.943 ± 0.041 (0.887)
iter. 2	0.947 ± 0.033 (0.895)***	0.947 ± 0.034 (0.903)***	0.951 ± 0.044 (0.914)	0.948 ± 0.042 (0.899)***
iter. 3	0.945 ± 0.036 (0.904)***	0.955 ± 0.028 (0.917)	0.953 ± 0.028 (0.919)***	0.951 ± 0.047 (0.912)
iter. 4	0.952 ± 0.028 (0.916)***	0.952 ± 0.033 (0.915)***	0.958 ± 0.028 (0.932)	0.957 ± 0.027 (0.919)
iter. 5	0.956 ± 0.028 (0.924)***	0.956 ± 0.029 (0.914)***	0.960 ± 0.027 (0.936)	0.956 ± 0.042 (0.917)***
data pool	0.967 ± 0.023 (0.945)			

Best result in a row according to the mean is indicated in bold. Value in parentheses denotes the 5th percentile.

* $p < 0.05$, ** $p < 0.01$, *** $p < 0.001$.

TABLE 5: RVE for models trained using the investigated query strategies over five active learning iterations.

	UVS	RVS	USS	RSS
initial		7.87 ± 10.0 (23.32)		
iter. 1	5.58 ± 8.95 (13.66)	6.94 ± 5.91 (17.64)***	11.62 ± 16.1 (26.97)***	8.05 ± 12.18 (19.96)***
iter. 2	5.1 ± 6.04 (13.69)	6.15 ± 6.73 (13.57)***	5.51 ± 15.96 (10.63)**	7.7 ± 13.25 (18.74)***
iter. 3	7.14 ± 8.94 (16.88)***	4.19 ± 5.13 (11.08)	6.16 ± 6.5 (14.8)***	7.32 ± 17.1 (14.89)***
iter. 4	6.06 ± 6.93 (12.44)***	5.12 ± 5.11 (11.79)	5.19 ± 7.81 (10.17)	5.25 ± 6.66 (11.11)
iter. 5	5.1 ± 6.84 (10.56)***	4.81 ± 5.25 (10.22)***	3.98 ± 6.97 (9.07)	6.04 ± 16.23 (10.97)***
data pool	3.8 ± 4.96 (7.6)			

Best result in a row according to the mean is indicated in bold. Value in parentheses denotes the 95th percentile.

* $p < 0.05$, ** $p < 0.01$, *** $p < 0.001$.

TABLE 6: MSD for models trained using the investigated query strategies over five active learning iterations.

	UVS	RVS	USS	RSS
initial			2.94 ± 3.9 (6.94)	
iter. 1	2.1 ± 1.9 (4.06)	2.17 ± 1.44 (4.88)**	2.81 ± 4.43 (6.41)***	2.28 ± 3.52 (4.84)
iter. 2	1.85 ± 1.29 (3.56)	1.86 ± 1.81 (3.6)	1.96 ± 4.89 (3.04)***	2.04 ± 4.3 (3.5)***
iter. 3	2.12 ± 2.45 (3.96)***	1.64 ± 1.5 (3.11)	1.64 ± 1.26 (3.2)**	2.05 ± 4.87 (3.0)
iter. 4	1.69 ± 1.15 (2.94)***	1.68 ± 1.27 (3.09)***	1.52 ± 1.66 (2.48)	1.58 ± 1.55 (2.75)
iter. 5	1.59 ± 1.27 (3.16)***	1.58 ± 1.26 (3.06)***	1.4 ± 1.44 (2.39)	1.73 ± 4.23 (2.87)**
data pool			1.18 ± 1.1 (2.03)	

Best result in a row according to the mean is indicated in bold. Value in parentheses denotes the 95th percentile.

* $p < 0.05$, ** $p < 0.01$, *** $p < 0.001$.

TABLE 7: HD for models trained using the investigated query strategies over five active learning iterations.

	UVS	RVS	USS	RSS
initial			36.3 ± 20.9 (80.2)	
iter. 1	32.1 ± 16.9 (61.8)	32.1 ± 15.3 (60.5)	36.4 ± 26.0 (76.3)*	33.2 ± 23.5 (71.1)
iter. 2	29.9 ± 14.5 (63.8)	29.9 ± 15.6 (58.3)	29.6 ± 21.4 (54.6)	29.6 ± 22.0 (55.8)
iter. 3	32.4 ± 20.1 (72.3)***	29.5 ± 17.2 (57.1)	27.5 ± 12.8 (48.0)	29.5 ± 24.1 (59.7)
iter. 4	28.3 ± 13.3 (59.8)	28.7 ± 13.5 (59.5)	27.4 ± 13.9 (53.3)	27.9 ± 16.5 (58.0)
iter. 5	28.5 ± 13.8 (56.7)***	28.6 ± 14.0 (62.3)***	25.6 ± 15.0 (46.6)	28.2 ± 20.9 (52.6)***
data pool			22.9 ± 12.7 (39.1)	

Best result in a row according to the mean is indicated in bold. Value in parentheses denotes the 95th percentile.

* $p < 0.05$, ** $p < 0.01$, *** $p < 0.001$.

TABLE 8: Evaluation results for the converged models.

	DICE	RVE [%]	MSD [mm]	HD [mm]
UVS	0.959 ± 0.027 (0.930)***	4.67 ± 6.23 (9.78)*	1.45 ± 1.18 (2.73)***	27.0 ± 12.4 (54.8)***
RVS	0.959 ± 0.035 (0.927)***	4.41 ± 5.33 (9.90)	1.44 ± 1.42 (2.63)***	26.4 ± 13.2 (55.4)***
USS	0.964 ± 0.025 (0.946)	4.20 ± 6.63 (8.30)	1.35 ± 2.94 (1.92)	23.4 ± 19.0 (38.4)
RSS	0.959 ± 0.029 (0.927)***	5.00 ± 6.44 (11.38)***	1.54 ± 1.94 (2.70)***	27.1 ± 16.1 (52.0)***
data pool	0.967 ± 0.023 (0.945)	3.80 ± 4.96 (7.60)	1.18 ± 1.10 (2.03)	22.9 ± 12.7 (39.1)

Best result for given metric according to the mean is indicated in bold (model trained on the whole data pool is excluded from comparison).

* $p < 0.05$, ** $p < 0.01$, *** $p < 0.001$.

TABLE 9: Quantile regression results quantifying the effect of uncertainty vs random sampling and slice vs volume sampling on the 5th percentile of DICE and 95th percentile of RVE, MSD, and HD. The analysis was run using evaluation results of the converged models.

	DICE [†]		RVE [%] [‡]		MSD [mm] [‡]		HD [mm] [‡]	
	coefficient	p-value	coefficient	p-value	coefficient	p-value	coefficient	p-value
Intercept	0.920 [0.914, 0.925]	<0.001	11.21 [9.26, 13.16]	<0.001	2.90 [2.64, 3.16]	<0.001	59.6 [50.0, 69.3]	<0.001
Uncertainty Sampling	0.012 [0.005, 0.019]	<0.001	-1.90 [-4.21, 0.42]	0.1	-0.41 [-0.73, -0.08]	0.015	-4.8 [-16.3, 6.6]	0.4
Slice Sampling	0.012 [0.005, 0.019]	<0.001	-0.80 [-3.12, 1.51]	0.5	-0.48 [-0.81, -0.16]	0.004	-7.7 [-19.1, 3.7]	0.2

Results from 0.05(†), 0.95(‡) quantile regression. Values in brackets denote 95% confidence interval.

random counterpart (RSS).

As our strategy relies on the model’s uncertainty to query cases, the confidence calibration of a model can have a substantial impact on which cases are deemed uncertain. Recently, it has been shown that modern deep neural networks do not output well-calibrated probabilities and tend to be overconfident [28]. In our work, we have used MC dropout that improves the calibration quality of models trained with the Dice loss [22]. Exemplary probability maps produced by our model are shown in Fig. 4. We think that investigation of various calibration techniques, e.g., deep ensembles and temperature scaling, in the context of active learning could be an interesting future research direction.

In our study, we focused on a detailed investigation of the proposed query strategy and we didn’t intend to achieve state-of-the-art results on the CT liver segmentation task. We are aware that in addition to using more training data, increasing model capacity or changing the architecture could further boost the segmentation performance. The influence of various neural network designs on the efficiency of our proposed query strategy would in our opinion make a compelling experiment. Moreover, we think that investigation of active learning together with AutoML frameworks such as nnU-net [29], which make state-of-the-art segmentation accessible to people without ML expertise, would be an interesting extension of our work.

Limitations Our conclusions are based on the assumption w.r.t. the annotation effort derived from empirical observations of annotation workflows. These assumptions might not hold for some annotators or if different labeling tools are used.

ACKNOWLEDGMENT

We would like to thank our clinical partners from Yokohama City University, Yokohama, Japan, Städtisches Klinikum Dresden, Dresden, Germany, and Radboud University Clinical Center, Nijmegen, the Netherlands for providing imaging data used in this study. We acknowledge the organizers of the LiTS and the CHAOS competitions for making the training data publicly available. We are thankful to Christiane Engel and Andrea Koller for providing manual segmentations. The work was funded by the Fraunhofer-Gesellschaft.

REFERENCES

- [1] Michela Antonelli, Annika Reinke, Spyridon Bakas, Keyvan Farahani, Bennett A Landman, Geert Litjens, Bjoern Menze, Olaf Ronneberger, Ronald M Summers, Bram van Ginneken, et al. The medical segmentation decathlon. arXiv preprint arXiv:2106.05735, 2021.
- [2] Hrvoje Bogunović, Freerk Venhuizen, Sophie Klimscha, Stefanos Apostolopoulos, Alireza Bab-Hadiashar, Ulas Bagci, Mirza Faisal Beg, Loza Bekalo, Qiang Chen, Carlos Ciller, et al. Retouch: The retinal oct fluid detection and segmentation benchmark and challenge. *IEEE transactions on medical imaging*, 38(8):1858–1874, 2019.
- [3] Patrick Bilic, Patrick Ferdinand Christ, Eugene Vorontsov, Grzegorz Chlebus, Hao Chen, Qi Dou, Chi-Wing Fu, Xiao Han, Pheng-Ann Heng, Jürgen Hesser, et al. The liver tumor segmentation benchmark (lits). arXiv preprint arXiv:1901.04056, 2019.
- [4] Eli Gibson, Yipeng Hu, Nooshin Ghavami, Hashim U Ahmed, Caroline Moore, Mark Emberton, Henkjan J Huisman, and Dean C Barratt. Inter-site variability in prostate segmentation accuracy using deep learning. In *International Conference on Medical Image Computing and Computer-Assisted Intervention*, pages 506–514. Springer, 2018.
- [5] Neerav Karani, Krishna Chaitanya, Christian Baumgartner, and Ender Konukoglu. A lifelong learning approach to brain mr segmentation across scanners and protocols. In *International Conference on Medical Image Computing and Computer-Assisted Intervention*, pages 476–484. Springer, 2018.
- [6] David A Cohn, Zoubin Ghahramani, and Michael I Jordan. Active learning with statistical models. *Journal of artificial intelligence research*, 4:129–145, 1996.
- [7] Keze Wang, Dongyu Zhang, Ya Li, Ruimao Zhang, and Liang Lin. Cost-effective active learning for deep image classification. *IEEE Transactions on Circuits and Systems for Video Technology*, 27(12):2591–2600, 2016.
- [8] Marc Gorriz, Axel Carlier, Emmanuel Faure, and Xavier Giro-i Nieto. Cost-effective active learning for melanoma segmentation. arXiv preprint arXiv:1711.09168, 2017.
- [9] Ozan Sener and Silvio Savarese. Active learning for convolutional neural networks: A core-set approach. arXiv preprint arXiv:1708.00489, 2017.
- [10] Lin Yang, Yizhe Zhang, Jianxu Chen, Siyuan Zhang, and Danny Z Chen. Suggestive annotation: A deep active learning framework for biomedical image segmentation. In *International conference on medical image computing and computer-assisted intervention*, pages 399–407. Springer, 2017.
- [11] Asim Smailagic, Pedro Costa, Hae Young Noh, Devsh Walawalkar, Kartik Khandelwal, Adrian Galdran, Mostafa Mirshekari, Jonathon Fagert, Susu Xu, Pei Zhang, et al. Medal: Accurate and robust deep active learning for medical image analysis. In 2018 17th IEEE international conference on machine learning and applications (ICMLA), pages 481–488. IEEE, 2018.
- [12] Samarth Sinha, Sayna Ebrahimi, and Trevor Darrell. Variational adversarial active learning. In *Proceedings of the IEEE/CVF International Conference on Computer Vision*, pages 5972–5981, 2019.
- [13] Özgün Çiçek, Ahmed Abdulkadir, Soeren S Lienkamp, Thomas Brox, and Olaf Ronneberger. 3d u-net: learning dense volumetric segmentation from sparse annotation. In *International conference on medical image computing and computer-assisted intervention*, pages 424–432. Springer, 2016.
- [14] Olaf Ronneberger, Philipp Fischer, and Thomas Brox. U-net: Convolutional networks for biomedical image segmentation. In *International Conference on Medical image computing and computer-assisted intervention*, pages 234–241. Springer, 2015.
- [15] Sergey Ioffe and Christian Szegedy. Batch normalization: Accelerating deep network training by reducing internal covariate shift. In *International conference on machine learning*, pages 448–456. PMLR, 2015.
- [16] Nitish Srivastava, Geoffrey Hinton, Alex Krizhevsky, Ilya Sutskever, and Ruslan Salakhutdinov. Dropout: a simple way to prevent neural networks from overfitting. *The journal of machine learning research*, 15(1):1929–1958, 2014.
- [17] Carole H Sudre, Wenqi Li, Tom Vercauteren, Sebastien Ourselin, and M Jorge Cardoso. Generalised dice overlap as a deep learning loss function for highly unbalanced segmentations. In *Deep learning in medical image analysis and multimodal learning for clinical decision support*, pages 240–248. Springer, 2017.
- [18] Abhijit Guha Roy, Sailesh Conjeti, Nassir Navab, and Christian Wachinger. Inherent brain segmentation quality control from fully convnet monte carlo sampling. In *International Conference on Medical Image Computing and Computer-Assisted Intervention*, pages 664–672. Springer, 2018.
- [19] Jishnu Mukhoti and Yarin Gal. Evaluating bayesian deep learning methods for semantic segmentation. arXiv preprint arXiv:1811.12709, 2018.
- [20] Yarin Gal and Zoubin Ghahramani. Dropout as a bayesian approximation: Representing model uncertainty in deep learning. In *International conference on machine learning*, pages 1050–1059. PMLR, 2016.
- [21] Alex Kendall and Yarin Gal. What uncertainties do we need in bayesian deep learning for computer vision? arXiv preprint arXiv:1703.04977, 2017.
- [22] Alireza Mehrtash, William M Wells, Clare M Tempany, Purang Abolmaesumi, and Tina Kapur. Confidence calibration and predictive uncertainty estimation for deep medical image segmentation. *IEEE transactions on medical imaging*, 39(12):3868–3878, 2020.
- [23] Grzegorz Chlebus, Hans Meine, Smita Thoduka, Nasreddin Abolmaali, Bram Van Ginneken, Horst Karl Hahn, and Andrea Schenk. Reducing inter-observer variability and interaction time of mr liver volumetry by combining automatic cnn-based liver segmentation and manual corrections. *PLoS one*, 14(5):e0217228, 2019.
- [24] A. Emre Kavur, N. Sinem Gezer, Mustafa Barış, Sinem Aslan, Pierre-Henri Conze, Vladimir Groza, Duc Duy Pham, Soumick Chatterjee, Philipp Ernst, Savaş Özkan, Bora Baydar, Dmitry Lachinov, Shuo Han, Josef Pauli, Fabian Isensee, Matthias Perkonig, Rachana Sathish, Ronnie Rajan, Debdoot Sheet, Gurbandurdy Dovletov, Oliver Speck, Andreas Nürnberg, Klaus H. Maier-Hein, Gözde Bozdağı Akar, Gözde Ünal, Oğuz Dicle, and M. Alper Selver. CHAOS Challenge - combined (CT-MR) healthy abdominal organ segmentation. *Medical Image Analysis*, 69:101950, April 2021.
- [25] Andrea Schenk, Guido PM Prause, and Heinz-Otto Peitgen. Local-cost computation for efficient segmentation of 3d objects with live wire. In *Medical Imaging 2001: Image Processing*, volume 4322, pages 1357–1364. International Society for Optics and Photonics, 2001.
- [26] Abhinav Shrivastava, Abhinav Gupta, and Ross Girshick. Training region-based object detectors with online hard example mining. In *Proceedings of the IEEE conference on computer vision and pattern recognition*, pages 761–769, 2016.
- [27] Cheng Bian, Xin Yang, Jianqiang Ma, Shen Zheng, Yu-An Liu, Reza Nezafat, Pheng-Ann Heng, and Yefeng Zheng. Pyramid network with online hard example mining for accurate left atrium segmentation. In *International workshop on statistical atlases and computational models of the heart*, pages 237–245. Springer, 2018.
- [28] Chuan Guo, Geoff Pleiss, Yu Sun, and Kilian Q Weinberger. On calibration of modern neural networks. In *International Conference on Machine Learning*, pages 1321–1330. PMLR, 2017.
- [29] Fabian Isensee, Paul F Jaeger, Simon AA Kohl, Jens Petersen, and Klaus H Maier-Hein. nnu-net: a self-configuring method for deep learning-based biomedical image segmentation. *Nature methods*, 18(2):203–211, 2021.